Lipids

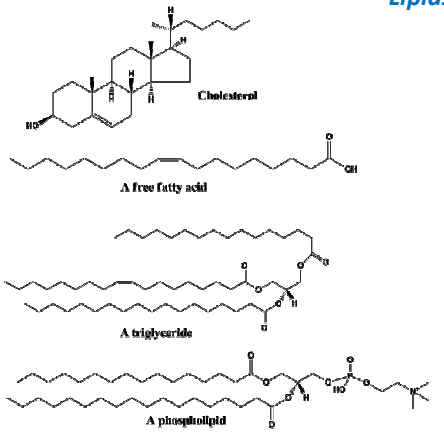

By Lmaps

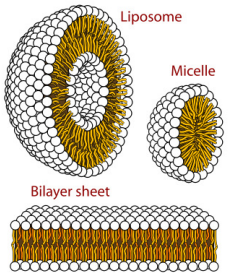

By Mariana Ruiz Villarreal

Encapsulation – essential for life

Evolving chemical systems require compartments for Darwinian evolution – to compete, to store information and to concentrate reactants/metabolites

Encapsulation into membranes is considered an early stage in prebiotic chemical evolution and essential requirement for the emergence of life

Formation of membranes is most easy to explain among major cellular components of the prebiotic Earth.
Many amphiphilic organic compounds spontaneously form vesicles in water at sufficiently high concentrations

The vesicle will encapsulate an aqueous solution inside a thin layer of organic material

Levine, R.M., Pearce, T.R., Adil, M., Kokkoli, E. Langmuir, 2013, 29 (29): 9208–9215.

Encapsulation – essential for life

Modern biological membranes consist primarily of phospholipids with embedded transmembrane proteins. Characterized by low permeability – a disadvantage during early evolution

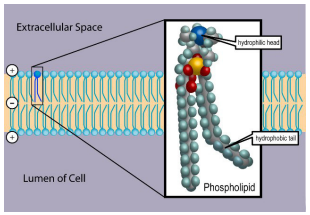

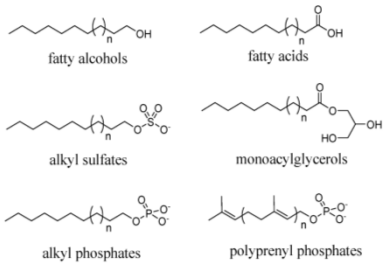

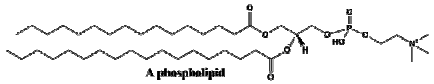

Fatty acids and fatty alcohols are likely prebiotic lipids

Spontaneous generation of lipid vesicles

The first protocell membranes may have assembled from fatty acids and related single-chain lipids available in the prebiotic environment.

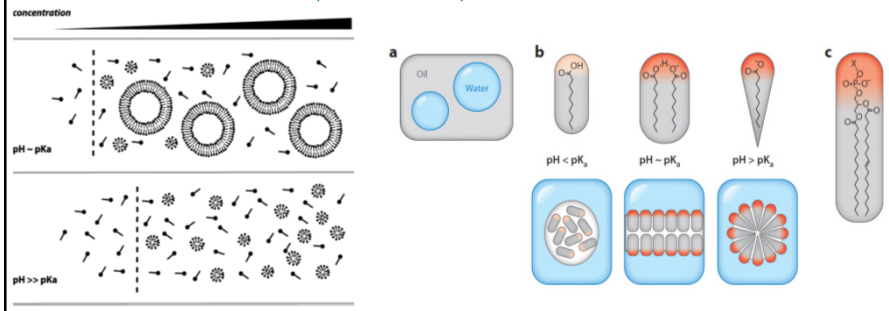

At different concentrations, fatty acids can partition between several different phases, including soluble monomers, micelles, and lamellar vesicles, with higher concentrations favoring larger vesicle aggregates.

I. Budin, A. Debnath, J. W. Szostak *J. Am. Chem. Soc.*, **2012**, 134, 20812-20819

Coupled growth and division of model protocell membranes

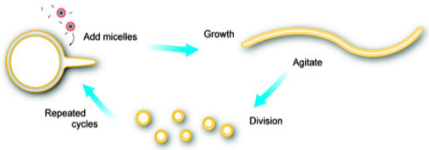

The growth of large multilamellar fatty acid vesicles fed with fatty acid micelles, in a solution where solute permeation across the membranes is slow, results in the transformation of initially spherical vesicles into long thread-like vesicles, a process driven by the transient imbalance between surface area and volume growth. Modest shear forces are then sufficient to cause the thread-like vesicles to divide into multiple daughter vesicles without loss of internal contents.

Ting F. Zhu, and Jack W. Szostak *J. Am. Chem. Soc.*, **2009**, 131 (15), 5705-5713

Coupled growth and division of model protocell membranes

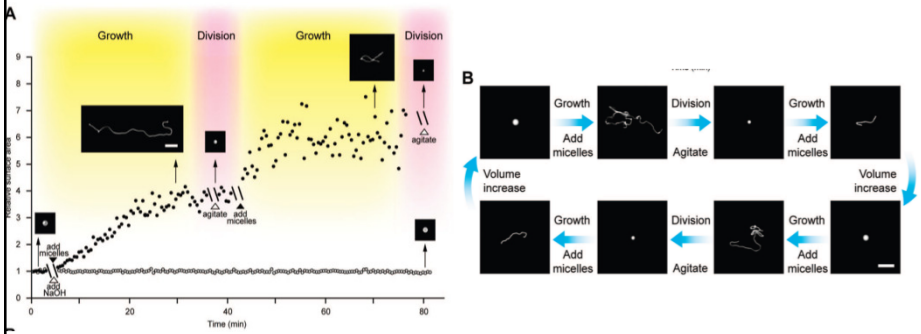

Cycles of vesicle growth and division. (A) Relative surface area after two cycles of addition of 5 equiv of oleate micelles (solid circles) or 5 equiv of NaOH (open circles) to oleate vesicles, each followed by agitation. Inset micrographs show vesicle shapes at indicated times. Scale bar, 10 μm. (B) Vesicle shapes during cycles of growth and division in a model prebiotic buffer (0.2 M Na-glycine, pH 8.5, ~1 mM initial oleic acid, vesicles contain 10 mM HPTS for fluorescence imaging). Scale bar, 20 μm.

Ting F. Zhu, and Jack W. Szostak *J. Am. Chem. Soc.*, **2009**, 131 (15), 5705-5713

Coupled growth and division of model protocell membranes

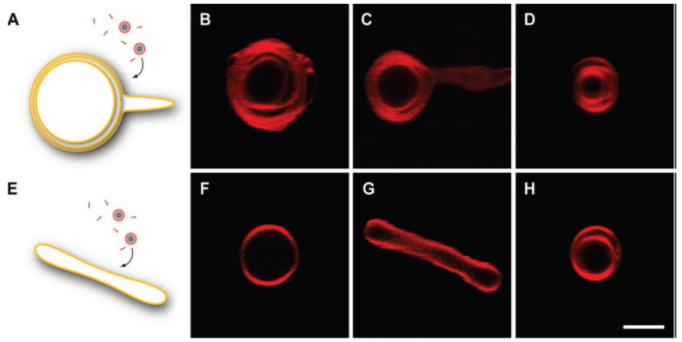

Growth of multilamellar versus unilamellar vesicles (A) Schematic diagram of incorporation of micelles into a multilamellar vesicle: the outermost membrane grows faster than the inner membrane layers. (B, C) Confocal images of multilamellar oleate vesicle (0.2 mol % Rh-DHPE, in 0.2 M Na-bicine, pH 8.5, ~1 mM initial oleic acid) before and 10 min after the addition of 1 equiv of oleate micelles, respectively. (D) Confocal image of multilamellar vesicle after division. (E) Schematic diagram of incorporation of micelles into a unilamellar vesicle. (F, G) Confocal images of unilamellar oleate vesicle (conditions as above) before and 10 min after the addition of 1 equiv of oleate micelles, respectively. (H) Confocal image of a multilamellar vesicle formed after the agitation of elongated unilamellar vesicles. Scale bar for B-D, F-H; 2 μm.

Ting F. Zhu, and Jack W. Szostak *J. Am. Chem. Soc.*, **2009**, 131 (15), 5705-5713

Coupled growth and division of model protocell membranes

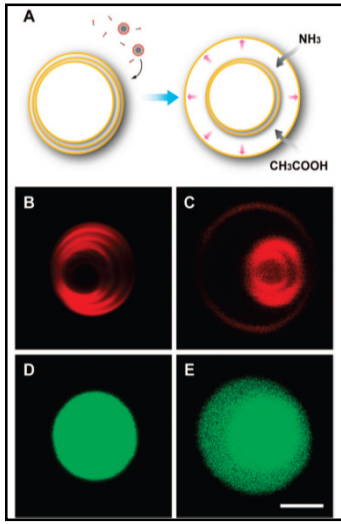

Vesicle growth in a highly permeable buffer (A) Schematic diagram of growth of a multilamellar vesicle in ammonium acetate: as the surface area of the outermost membrane increases, the solutes in their neutral forms (NH_3 and CH_3COOH) permeate the membrane, allowing the internal volume to increase. (B, C) Confocal images of multilamellar oleate vesicle (0.2 mol % Rh-DHPE, in 0.2 M ammonium acetate, pH 8.5, ~1 mM initial oleic acid) before and 10 min after the addition of 1 equiv of oleate micelles, respectively. (D, E) Confocal images of multilamellar oleate vesicle (containing 2 mM HPTS, in 0.2 M ammonium acetate, pH 8.5, ~1 mM initial oleic acid) before and 10 min after the addition of 1 equiv of oleate micelles, respectively. Scale bar for B-E, 2 μm.

Ting F. Zhu, and Jack W. Szostak *J. Am. Chem. Soc.*, **2009**, 131 (15), 5705-5713

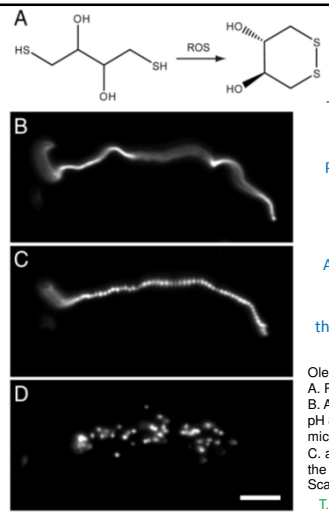

Photochemically driven protocell division

The illumination of filamentous fatty acid vesicles rapidly induces pearling and subsequent division in the presence of thiols.

Photochemically generated reactive oxygen species oxidize thiols to disulfide-containing compounds that associate with fatty acid membranes, inducing a change in surface tension and causing pearling and subsequent division.

Alternative route for the emergence of early self-replicating cell-like structures, particularly in thiol-rich surface environments.
The subsequent evolution of cellular metabolic processes controlling the thiol:disulfide redox state would have enabled autonomous cellular control of the timing of cell division, a major step in the origin of cellular life.

Oleate vesicle pearling and division.
A. Radical-mediated oxidation of DTT.
B. An oleate vesicle (containing 2 mM HPTS, in 0.2 M Na-glycinamide, pH 8.5, 10 mM DTT) 30 min after the addition of five equivalents of oleate micelles.
C. and D. Under intense illumination (for 2 s and 12 s, respectively), the long thread-like vesicle went through pearling and division
Scale bar, 10μm.

T. F. Zhu, K. Adamala, N. Zhang, J. W. Szostak *PNAS*, **2012**, doi:10.1073/pnas.1203212109

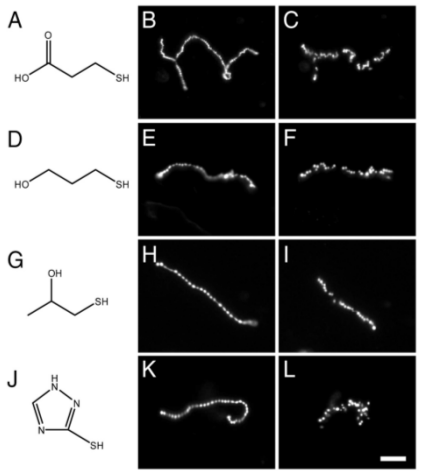

Photochemically driven protocell division

Oleate vesicle pearling and division with various thiols in the solution.

(A) 3-mercaptopropionic acid.
(B and C) An oleate vesicle (containing 2 mM HPTS, in 0.2 M Na-bicine, pH 8.5, 10 mM 3-mercaptopropionic acid, 30 min after the addition of five equivalents of oleatemicelles) went through pearling and division under intense illumination (for 3 s and 15 s, respectively).

(D) 3-mercapto-1-propanol.
(E and F) An oleate vesicle as above but in 50 mM 3-mercapto-1-propanol, went through pearling and division under intense illumination (for 2 s and 10 s, respectively).

(G) 1-mercapto-2-propanol.
(H and I) An oleate vesicle as above but in 50 mM 1-mercapto-2-propanol went through pearling and division under intense illumination (for 2 s and 9 s, respectively).

(J) 3-mercapto-1,2,4-triazole.
(K and L) An oleate vesicle as above but in 50 mM 3-mercapto-1,2,4-triazole went through pearling and division under intense illumination (for 3 s and 13 s, respectively).
Scale bar, 20 μm.

T. F. Zhu, K. Adamala, N. Zhang, J. W. Szostak *PNAS*, **2012**, doi:10.1073/pnas.1203212109

Transition: Micelles-Vesicles-Protocells

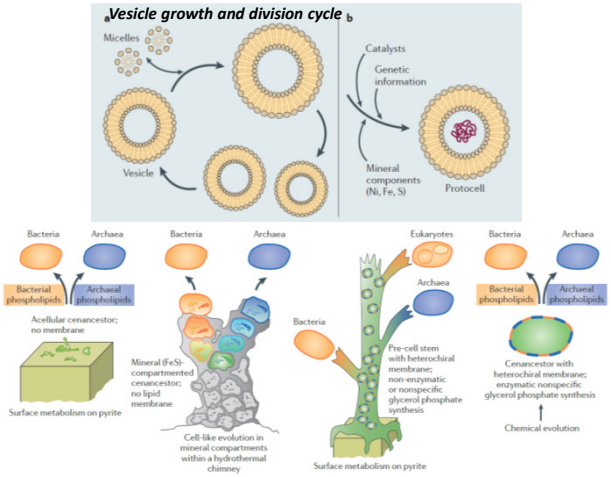

Encapsulation – essential for life

Fatty acids have been found in meteorites – plausible prebiotic synthesis pathways existed in the early Solar System

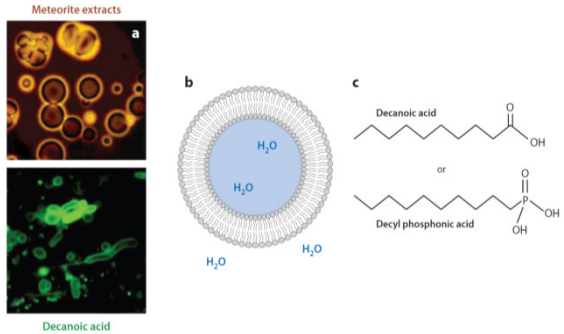

Extracts of meteorites containing these compounds spontaneously form vescicles when hydrated

Fischer-Tropsch synthesis

Long hydrocarbon chains from CO + H_2 in presence of metal catalysts and high pressure, fatty acids and alcohols are minor by-products

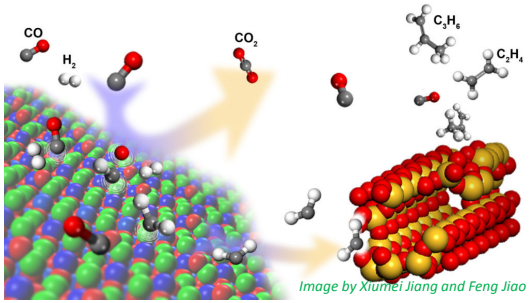

Image by Xiumei Jiang and Feng Jiao

The mixture of D_2 and CO over meteoritic iron or iron ore produced alkanes and n-fatty acids

Oro, J. et al. Geochim. Cosmochim. Acta **1976**, *40*, 915-924.

Fischer-Tropsch synthesis

Main reactions	
1. Paraffins	$(2n+1)H_2+nCO \rightarrow C_nH_{2n+2}+nH_2O$
2. Olefins	$2nH_2+nCO \rightarrow C_nH_{2n}+nH_2O$
Side reactions	
3. Water-Gas-Shift (WGS)	$CO+H_2O \leftrightarrow CO_2+H_2$
4. Carbide formation	$yC + xM \leftrightarrow M_xC_y$
5. Alcohols	$2nH_2+nCO \rightarrow C_nH_{2n}+2O+(n-1)H_2O$
6. Boudouard reaction	$2CO \rightarrow C+CO_2$
7. Catalyst reduction and oxidation	$M_xO_y + yH_2 \leftrightarrow xM + yH_2O$ $M_xO_y + yCO \leftrightarrow xM + yCO_2$
8. Coking	$H_2 + CO \rightarrow C + H_2O$

Hydrothermal Fischer-Tropsch synthesis

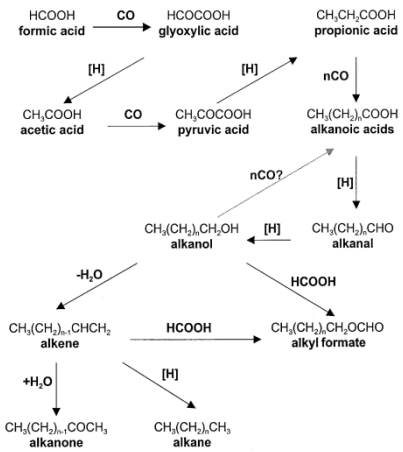

Formic or oxalic acid heated in water at 150-250^{0}C (stainless steel reactor) yielded a mixture of C_{12}-C_{33} lipids

Rushdi, A., Simoneit B. Origins Life Evol. Biospheres **2001**, *31*, 103-118

When CO, H_2 and NH_3 are allowed to react at 200-700^{0}C in presence of Ni, Al, or clay catalysts, aminoacids are detected:
glycine, alanine, sarcosine, aspartic acid, glutamic acid, arginine, histidine, lysine and ornithine

Yoshino, D.; Hayatsu, R.; Anders, E. *Geochim. Cosmochim. Acta* **1971**, *35*, 927-938

Prebiotic prenyl lipids

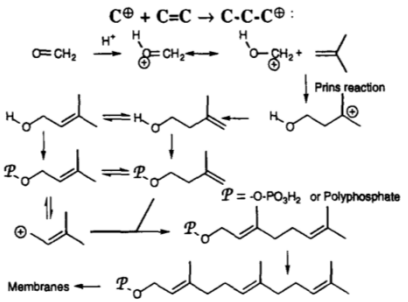

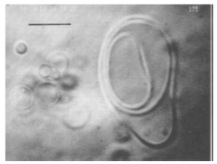

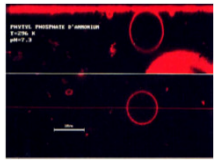

Ourisson, G. et al. Angew. Chem. Int. Ed. **1996**, *35*, 177-180
Ourisson, G.; Nakatani, Y. *Tetrahedron* **1999**, *55*, 3183-3190

Prins reaction

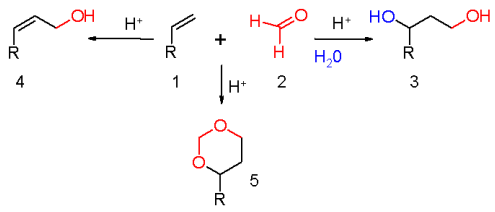

Extraterrestrial origin of biomolecules

Murchison meteorite
chondrite

Table 1. Soluble Organic Compounds in the Murchison Meteorite[a]

class of compounds	parts per million	n^b
aliphatic hydrocarbons	>35	140
aromatic hydrocarbons	15–28	87
polar hydrocarbons	<120	10[d]
carboxylic acids	>300	48[d]
amino acids	60	75[d]
imino acids	nd[c]	10
hydroxy acids	15	7
dicarboxylic acids	>30	17[d]
dicarboximides	>50	2
pyridinecarboxylic acids	>7	7
sulfonic acids	67	4
phosphonic acids	2	4
N-heterocycles	7	31
amines	13	20[d]
amides	nd[c]	27
polyols	30	19

Nucleolipids – a replication mechanism for genetic information?

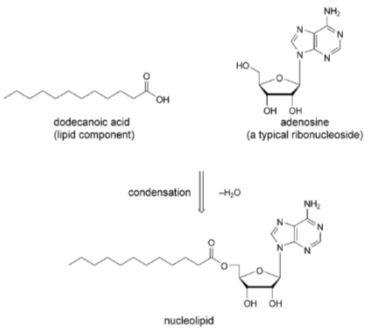

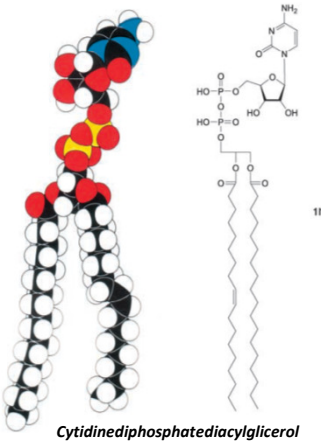

Cytidinediphosphatediacylglicerol

Antibiotic nucleolipids

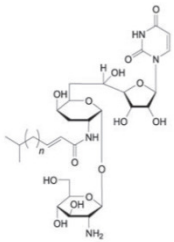

2 Tunicamycin A $n = 9$
3 Tunicamycin B $n = 10$
4 Tunicamycin C $n = 8$
5 Tunicamycin D $n = 11$

from *Streptomyces lysosuperficus*

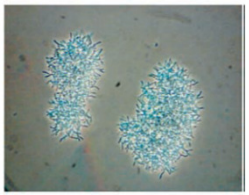

Streptomyces lysosuperficus

Inhibit peptidoglycan synthesis

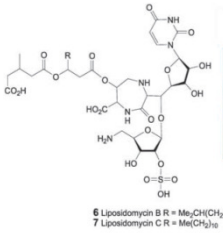

6 Liposidomycin B R = $Me_2CH(CH_2)_8$
7 Liposidomycin C R = $Me(CH_2)_{10}$

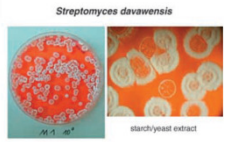

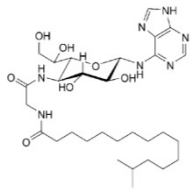

Septacidine (**8**)
from *Streptomyces fimbriatus*

Nucleolipids – a replication mechanism for genetic information?

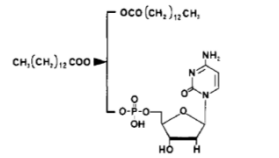

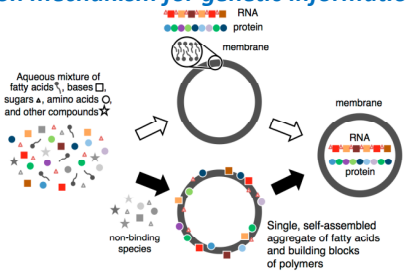

Black, R. A.; Blosser, M. C. *Life* **2016**, *6*(3), 33; doi:10.3390/life6030033

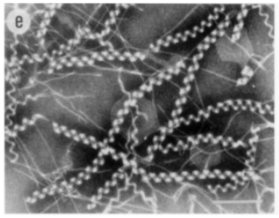

Scalebar: 200 nm

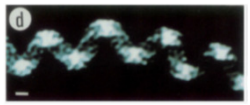

Scalebar: 10 nm

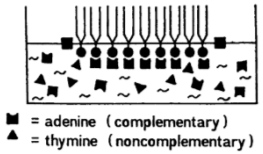

Yanagawa, H. et al. J. Am. Chem. Soc. **1989**, *111*, 4567-4570

Rosemeyer, H. Chem. Biodiversity **2005**, *2*, 977

Noncovalent nucleotide association with membranes

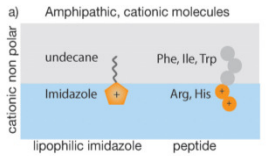

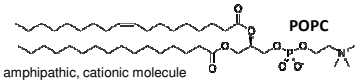

RNA localization with a model amphipathic, cationic molecule

a) Design of RNA-localizing molecules that include both nonpolar and cationic regions.
b) The change in zeta potential
c) Schematic of the FRET assay used to assess RNA localization to vesicle membranes
d) RNA (5'-FAM-U_{15} and 5'-FAM-A_{15}) shows increasing localization to POPC membranes that contain increased amounts of undecylimidazole.

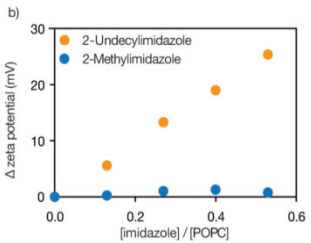

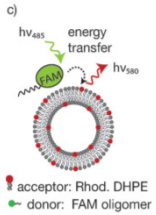

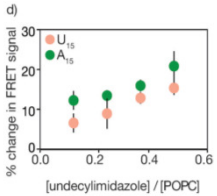

Neha P. Kamat, Sylvia Tobe, Ian T. Hill, and Jack W. Szostak *Angew. Chem. Int. Ed.* **2015**, *54*, 11735 –11739

Noncovalent nucleotide association with membranes

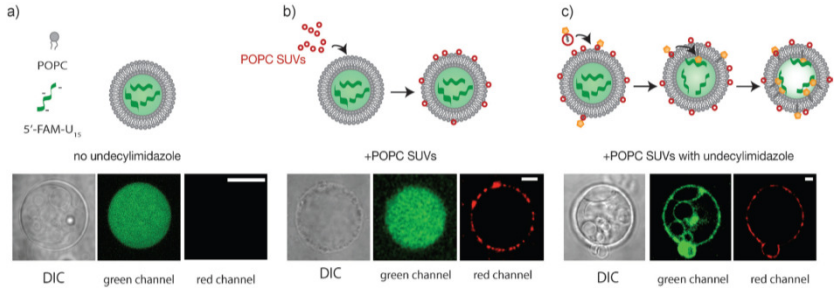

Microscopy of encapsulated RNA localization to POPC membranes with 2-undecylimidazole. Confocal images of 5'-FAM-U_{15} RNA (green) association with giant POPC vesicles membranes in the presence of 2-undecylimidazole. Differential interference contrast (DIC) microscopy images are shown for each vesicle.

a) RNA appears uniformly distributed in the interior of POPC GUVs.
b) The addition of SUVs containing a rhodamine-labeled lipid (red) leads to SUV aggregation and association with the giant vesicle membranes, but RNA (green) remains uniformly encapsulated in the vesicle interior.
c) The addition of SUVs containing a rhodamine-labeled lipid (red) and 40 mol% 2-undecylimidazole leads to SUV association with vesicle membranes and RNA (green) localizes to the vesicle surface. The scale bar is 20 mm.

SUV – small unilamellar vescile ***GUV – giant unilamellar vescile (5-25 µm)***

Neha P. Kamat, Sylvia Tobe, Ian T. Hill, and Jack W. Szostak *Angew. Chem. Int. Ed.* **2015**, *54*, 11735 –11739

Noncovalent nucleotide association with membranes

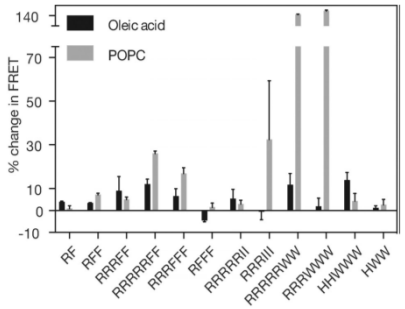

Peptide-induced RNA–membrane association. A FRET assay reports RNA localization (5'-FAM-U_{15}) to POPC and oleic acid membranes (7.5 mm) 10 h after the addition of 1 mm of various peptides to the vesicle solution at pH 8. Data is reported as a percentage change from control samples that lack peptide. n=4, error bars represent the standard error of the mean.

Neha P. Kamat, Sylvia Tobe, Ian T. Hill, and Jack W. Szostak *Angew. Chem. Int. Ed.* **2015**, *54*, 11735 –11739

Noncovalent nucleotide association with membranes

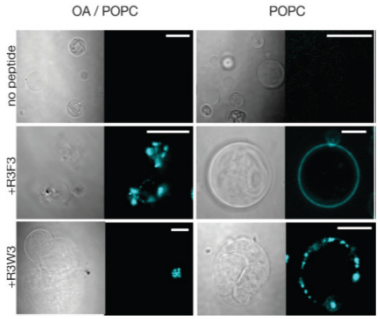

Microscopy of peptide-induced RNA–membrane association. Confocal images show RNA localization (5'-AlexaFluor647-labeled 15-mer, cyan) to the outside of oleic acid/POPC (90%/10%) and pure POPC membranes in the presence of R3F3 and R3W3 peptides. Control samples had no peptide added. For each image, the left panel shows the DIC image and the right panel shows AlexaFluor647 fluorescence. The scale bar is 20 mm.

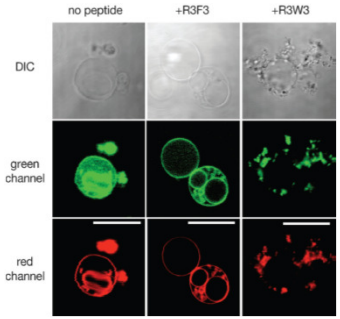

Microscopy of encapsulated RNA localization to POPC membranes with peptides. Confocal images show that RNA (5'-FAMU$_{15}$, green) encapsulated in POPC vesicles (containing a rhodaminelabeled lipid, red) becomes localized to the membrane of certain vesicles after an overnight incubation with R3F3 and R3W3 peptides. The scale bar is 20 mm.

Neha P. Kamat, Sylvia Tobe, Ian T. Hill, and Jack W. Szostak *Angew. Chem. Int. Ed.* **2015**, *54*, 11735 –11739

Phosphates

slice of the Gebel Kamil Meteorite with schreibersite rimmed by kamacite

Schreibersite is generally a rare iron-nickel phosphide mineral, $(Fe,Ni)_3P$, though common in iron-nickel meteorites

Acidic schreibersite corrosion under anaerobic conditions (10% aq. HCl/N_2) → soluble forms of phosphorus

$$(Fe,Ni)_3P + HCl_{aq} \rightarrow H_2PO_3^- \rightarrow H_2P_2O_5^{2-}$$

T. P. Kee *et al.Geochimica et Cosmochimica Acta.* ***2013*** *109,* 90-112

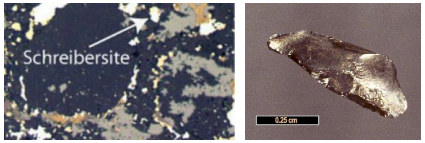

Virginia Smith, UA Lunar & Planetary Laboratory

Image of schreibersite grain present in a thin-section of the enstatite meteorite, KLE 98300.

Phosphates

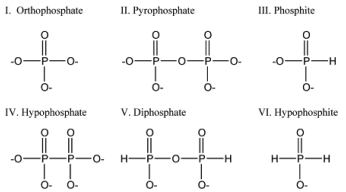

$$Fe_3P + 7H_2O \rightarrow Fe_3O_4 + H_3PO_3 + 5\tfrac{1}{2}H_2(g)$$
$$H_3PO_3 + H_2O \rightarrow H_3PO_4 + H_2(g)$$
$$2H_3PO_3 \rightarrow H_4P_2O_6 + H_2(g)$$
$$H_4P_2O_6 + H_2O \rightarrow H_4P_2O_7 + H_2(g)$$
$$H_4P_2O_7 + H_2O \rightarrow 2H_3PO_4$$

Radical pathway of the corrosion is suggested.
In presence of simple organic molecules (e.g. acetic acid) organophosphorous compounds are detected

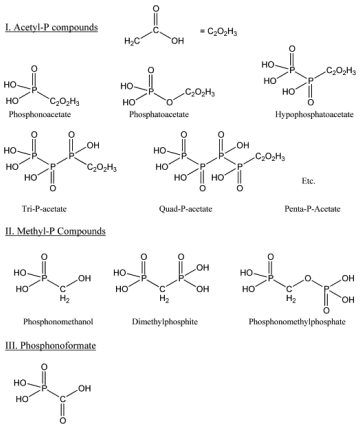

M. Pasek *et al.Geochimica et Cosmochimica Acta.* ***2007*** *71,* 1721-1736

Phospholipids

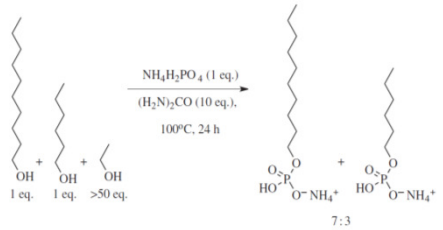

M. Powner, J. Sutherland *Phil. Trans. R. Soc. B* **2011**, *366*, 2870–2877

Lipids - summary

Many amphiphilic organic compounds spontaneously form vesicles in water at sufficiently high concentrations

Current phospholipid membranes likely evolved late. Protocells probably encapsulated by fatty acids, fatty alcohols, prenyl oligomers, or phosphorylated alcohols

Nucleolipids are proposed as intermediates in templated oligonucleotide replication

Phosphorus was accessible upon corrosion of meteorite materials and could be incorporated into lipids

The origin of small reactive intermediates

Wikimedia , Carles Millan

Schreibersite $(Fe,Ni)_3P$, from iron-nickel meteorites: source of phosphorus, iron and nickel

Under more neutral conditions phosphates recombine with iron → $Fe_3(PO_4)_2$ (**vivianite**)

It should be re-solubilized to become accessible for following chemical transformations

HCN – the crucial reactive intermediate – burning of carbon-rich chondrite meteorites into redox-neutral atmosphere containing N_2 and water

$$Fe_3(PO_4)_2 + 18CN^-_{aq} \rightarrow 2PO_4^{3-} + 3[Fe(CN)_6]^{4-}$$

Two important functions: solubilization of phosphates and concentration of atmospheric HCN deposited as salts of mono- and divalent cations (Na, K, Mg, Ca)

Similar reactions take place with insoluble copper and nickel sulfides deposited by iron-nickel meteorite impacts (same occurence as schreibersite, rich mining sources of these metals until today)

$$NiS + H_2O + 6CN^- \rightarrow [Ni(CN)_6]^{4-} + HS^- + OH^-$$

$$Cu_2S + H_2O + 6CN^- \rightarrow 2[Cu(CN)_3]^{2-} + HS^- + OH^-$$

The origin of small reactive intermediates

Thermal decomposition of cyanoferrates (volcanic):

$$(Na,K)_4[Fe(CN)_6] \xrightarrow{700^oC} 4(\mathbf{Na/K})\mathbf{CN} + Fe(CN)_2$$

$$3Fe(CN)_2 \xrightarrow{700^oC} Fe_3C + 5C + 3N_2$$

$$Fe(CN)_2 \xrightarrow{700^oC} Fe + 2C + N_2$$

$$Ca_2[Fe(CN)_6] \xrightarrow{660^oC} 2Ca(CN)_2 + Fe(CN)_2$$

$$Ca(CN)_2 \xrightarrow{660^oC} \mathbf{CaNCN} + C \xrightarrow{1000^oC} \mathbf{CaC_2} + N_2$$

$$Mg_2[Fe(CN)_6] \xrightarrow{315^oC} 2Mg(CN)_2 + Fe(CN)_2$$

$$Mg(CN)_2 \xrightarrow{395^oC} MgCN_2 + C$$

$$3MgCN_2 \xrightarrow{420^oC} \mathbf{Mg_3N_2} + 3C + 2N_2$$

$Cu_2S + H_2O + 6CN^- \rightarrow 2[Cu(CN)_3]^{2-} + HS^- + OH^-$

cyanocuprates and HS^- are delivered by this process

Photoredox cycle based on cyanocuprates may convert HCN into cyanogen

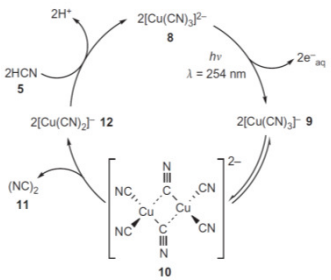

Action of water (bufferred to neutral or slightly acidic) on that mixture produced concentrated HCN solution + cyanamide (from CaNCN) + acetylene (from CaC_2) + ammonia (from Mg_3N_2)